Level-Spacing Distributions of Planar Quasiperiodic Tight-Binding Models

J. X. Zhong,[1,2] U. Grimm,[1] R. A. Römer,[1] and M. Schreiber [1]
[1] *Institut für Physik, Technische Universität Chemnitz, D-09107 Chemnitz, Germany*
[2] *Department of Physics, Xiangtan University, Xiangtan 411105, P. R. China*
(*Revision* : 1.13, printed February 1, 2008)

We study the statistical properties of energy spectra of two-dimensional quasiperiodic tight-binding models. We demonstrate that the nearest-neighbor level spacing distributions of these non-random systems are well described by random matrix theory. Properly taking into account the symmetries of models defined on various finite approximants of quasiperiodic tilings, we find that the underlying universal level-spacing distribution is given by the Wigner-Dyson distribution of the Gaussian orthogonal random matrix ensemble. Our data allow us to see the differences between the Wigner surmise and the exact level-spacing distribution. In particular, our result differs from the critical level-spacing distribution computed at the metal-insulator transition in the three-dimensional Anderson model of disorder.

PACS numbers: 71.23.Ft, 71.30.+h, 05.45.+b, 72.15.Rn

Following the pioneering works of Wigner and Dyson [1], random matrix theory (RMT) has been successfully applied to investigate a great variety of complex systems such as nuclear spectra, large atoms, mesoscopic solids, and chaotic quantum billiards [2–5]. In such systems, it has been shown that spectral fluctuations can be modeled by universal level-spacing distributions (LSD) such as, e.g., $P_{\rm GOE}(s)$ for the Gaussian orthogonal random matrix ensemble (GOE) [2].

A very natural application of RMT concerns disordered systems [6]. It has been shown that the metal-insulator transition (MIT) in the three-dimensional (3D) Anderson model of localization is accompanied by a transition of the LSD $P(s)$ [7–9]. Here, s denotes the energy spacing in units of the mean level spacing Δ. In the metallic regime, $P(s)$ closely follows the Wigner surmise $P_{\rm W}(s) = \pi s \exp(-\pi s^2/4)/2$, which is a good approximation of $P_{\rm GOE}(s)$. On the insulating side, $P(s)$ is given by Poisson's law $P_{\rm P}(s) = \exp(-s)$. One important difference between the two distributions is their small-s behavior: $P_{\rm W}(s \to 0) \approx \pi s/2$ and $P_{\rm P}(s \to 0) \approx 1$, indicating level repulsion and clustering, respectively. At the MIT, where the eigenstates are multifractal [10], another LSD, $P_c(s)$, has been observed [7–9].

Multifractal eigenstates — neither extended nor exponentially localized — have also been found in tight-binding (TB) models of quasicrystals. In fact, these seem predominant in 1D and 2D [11]; in 3D, the attainable system sizes are yet too small for definite statements [12]. The multifractality is assumed to be connected to the unusual transport properties of quasicrystals [13], e.g., their resistivity increases considerably with decreasing temperature and improving structural quality of the sample. Thus, one may speculate that the LSD in quasiperiodic models is also distinct from the Wigner and Poisson behavior.

Quasicrystals lack the translational symmetry of periodic crystals, but still retain long-range (orientational) order and show non-crystallographic symmetries incompatible with lattice periodicity. Thus, they constitute a class of materials somewhere in between perfect crystals and amorphous systems. Besides quasicrystals with icosahedral symmetry [14], which are aperiodic in any direction of the 3D space, also dodecagonal [15], decagonal [16], and octagonal [17] phases have been found, which can be viewed as periodic stacks of quasiperiodic planes with 12-, 10-, and 8-fold symmetry, respectively. Structure models of quasicrystals are based on quasiperiodic tilings which can be constructed, e.g., by projection from higher-dimensional periodic lattices [18]. We emphasize that such quasiperiodic tilings, albeit yielding perfect rotationally symmetric diffraction patterns, exhibit n-fold rotational symmetry in a generalized sense only. In particular, there need not be a point with respect to which the tiling has an *exact* global n-fold rotational symmetry. If such a point exists, it is unique.

In order to understand the transport properties of quasicrystals [13], TB models defined on such aperiodic tilings (notably the Penrose tiling) have received considerable attention [11,19–25]. For a TB model defined on the octagonal (Ammann-Beenker) tiling [26], the LSD has also been used to classify the spectrum [23–25]. For periodic approximants, level repulsion was observed [23,24], and $P(s)$ was argued to follow a log-normal distribution [24]. However, a calculation for finite patches with an exact 8-fold symmetry yielded level clustering [25].

In this Letter, we show that these somewhat diverging results become comprehensible when one realizes that the tilings of Refs. [23,24] still retain non-trivial symmetries, such as a reflection symmetry for the standard periodic approximants. In order to obtain the underlying universal LSD, one should consider the irreducible subspectra separately, or break the symmetry by, e.g., either choosing patches without symmetry, or imposing suitable boundary shapes as in quantum billiards, or introducing disorder. Properly taking this into account, we find that the underlying LSD of these non-random Hamiltonians

is neither $P_{\rm P}(s)$ [25], nor log-normal [24], nor $P_c(s)$ but rather $P_{\rm GOE}(s)$. The accuracy of our data further allows us to show that it is also not $P_{\rm W}(s)$ although this is as usual a reasonable approximation [2]. We emphasize that our results apply to all planar tilings mentioned above.

Let us reconsider [23–25] the octagonal tiling consisting of squares and rhombi with equal edge lengths as in Fig. 1(a). Besides the projection method mentioned above, one may also use the self-similarity of the tiling to construct ever larger patches by successive inflation steps [27]. E.g., the patch in Fig. 1(a) corresponds to two inflation steps of the inner shaded octagon. On this tiling, we define the Hamiltonian $H = \sum_{\langle i,j \rangle} |i\rangle\langle j|$ with free boundary conditions, $|i\rangle$ denotes the Wannier state at vertex i, and $\langle i,j \rangle$ runs over all pairs of vertices connected by an edge of unit length.

We diagonalize the Hamiltonian by standard methods, and study the LSD of the full spectrum. Due to the bipartiteness of the tiling, the energy spectrum is symmetric about $E = 0$. Furthermore, it has been shown that a finite fraction of the states are degenerate at $E = 0$ [19,22–24]. These correspond to confined states [19] limited to certain local environments, do not contribute to the LSD, and we neglect them. In agreement with previous calculations [23], we find that the integrated density of states (IDOS) is very smooth. This is different from 1D quasiperiodic systems which typically have singular continuous spectra [11]. Nevertheless, the IDOS is not strictly linear as required by RMT, so we "unfold" the spectrum by fitting the IDOS to a cubic spline [8] and use $s_i = N_{\rm av}(E_{i+1}) - N_{\rm av}(E_i)$ for the level-spacing at the ith level with $N_{\rm av}$ the smoothed IDOS. We remark that the unfolded LSD is not a bulk quantity since Δ^{-1} is proportional to the system size. In what follows, we shall always consider instead of $P(s)$ the integrated LSD $I(s) = \int_s^\infty P(t)dt$ which is numerically more stable [8,9].

Fig. 2(a) shows $I(s)$ obtained for a large octagonal patch with 157369 vertices corresponding to three more inflation steps of Fig. 1(a). At first glance, $I(s)$ seems to be close to the integrated Poisson law $I_{\rm P}(s) \equiv P_{\rm P}(s)$, as observed in Ref. [25]. However, this patch has the full D_8-symmetry of the regular octagon, hence the Hamiltonian matrix splits into ten blocks according to the irreducible representations of the dihedral group D_8: using the rotational symmetry, one obtains eight blocks, two of which split further under reflection, while the remaining six form three pairs with identical spectra. This gives a total of seven independent subspectra. As with the confined states, we neglected the exact degeneracies induced by symmetry in Fig. 2(a), since they only contribute to $P(0)$. The integrated LSD of the seven independent subspectra are shown in Fig. 2(b). Each subspectrum matches the integrated Wigner surmise $I_{\rm W}(s) = \exp(-\pi s^2/4)$ to very good accuracy. From RMT it is known [2] that the LSD of a superposition of k independent spectra, each of which obeys Wigner statistics, is given by $P_{\rm W}^{(k)}(s) = \frac{d^2}{ds^2}[\mathrm{erfc}(\frac{\sqrt{\pi}}{2}\frac{s}{k})]^k$ with $\mathrm{erfc}(t)$ the complementary error function. For large k, $P_{\rm W}^{(k)}(s)$ approaches the Poisson law $P_{\rm P}(s)$. In Fig. 1(a), we therefore also included the integrated LSD $I_{\rm W}^{(7)}(s)$ of $k = 7$ Wigner spectra. The data clearly fits this curve better than $I_{\rm P}(s)$. This explains why in a previous calculation [25] a Poisson-like distribution was found. We also note that our data do not follow the integrated LSD $I_c(s)$ found at the Anderson MIT [9].

Upon closer inspection of Fig. 2(b), we see that there are only very small differences between the seven integrated LSD, whereas there are slightly larger deviations to $I_{\rm W}(s)$. In Fig. 3, we show the small- and large-s behavior in more detail, restricting ourselves to data from one irreducible sector. We include data for patches of different sizes, corresponding to two, three, four, and five inflation steps of the inner shaded octagon of Fig. 1(a) with 833, 4713, 27137, and 157369 vertices, respectively. The convergence to $I_{\rm W}(s)$ with increasing patch size is apparent both for small and large s in Fig. 3. However, the above-mentioned small deviations from $I_{\rm W}(s)$ still persist, even though the finite-size dependence is already very small. Therefore, we also consider in Fig. 3 the *exact* integrated LSD $I_{\rm GOE}(s)$ [2]. Although the Wigner surmise is usually a sufficient approximation of the exact LSD, we show in the inset of Fig. 3 that our data follow the exact curve $I_{\rm GOE}(s)$. Thus, the small deviations seen in Fig. 2, are due to the differences between $I_{\rm W}(s)$ and $I_{\rm GOE}(s)$.

We can also approximate the octagonal tiling by patches which do not have exact symmetries. For instance, in Fig. 1(b) we show such a square-shaped patch cut out of the octagonal tiling. Although the quasiperiodic eightfold order is restored in the infinite patch, there is never any exact symmetry present in the finite approximants. The LSD is of the Wigner-type as shown in Fig. 2(c) for patches with side lengths $L = 40$, 60, and 80, corresponding to 1980, 4392, and 7785 vertices, respectively. Thus, contrary to the case of a simple square lattice exhibiting level clustering, we find level repulsion. Again, we observe small deviations from $I_{\rm W}(s)$ which can be explained as previously when using $I_{\rm GOE}(s)$. If one uses square-shaped approximants with symmetries, for instance squares centered around the eightfold point of the patch in Fig. 1(a) or the standard periodic approximants used in Refs. [23,24], the LSD is again a superposition of the LSD of the irreducible subspectra. Thus, approaching the infinite tiling by square-shaped patches only slightly shifted with respect to each other may give quite different LSD. We have obtained the same results also for circular patches. In this case, one can have either D_8, or reflection, or no symmetry, depending on the choice of the center. Thus, the LSD is well approximated by $P_{\rm W}^{(7)}(s)$, or $P_{\rm W}^{(2)}(s)$, or $P_{\rm W}^{(1)}(s) \equiv P_{\rm W}(s)$, respectively.

A different way of excluding any symmetries is given by choosing patches with special boundary shapes. In fact, this is well known in the context of quantum billiards where it has been used to construct quantum chaotic motion [4,5]. One of the most prominent examples is the Sinai billiard [4,5], which consists of 1/8 of a square and a circular arc centered in the midpoint of the square. Due to these boundary conditions, the LSD follows the Wigner surmise even for free electrons [4] instead of a Poisson law which is found for integrable motion in simple square or circular billiards [2]. In Fig. 1(c), we show a Sinai billiard-shaped cut of the octagonal tiling. Moving Sinai's billiard table across the octagonal tiling, we can now generate many different patches. However, in contrast to the square-shaped boundary, we never find a case that retains any of the D_8-symmetries. We computed $I(s)$ for quasiperiodic billiards with $L = 70$, 80, 90, 100, and 110, corresponding to patches with 2416, 3146, 3969, 4892, and 5905 vertices, respectively. The results presented in Fig. 2(d) follow $I_{\rm W}(s)$, and, again, are even closer to $I_{\rm GOE}(s)$.

We emphasize that, apart from statistical fluctuations at small and large values of s as shown in Fig. 3, there is no systematic size-dependence of $I(s)$. This is in contrast to the 2D Anderson model at weak disorder [28], where a qualitative change towards Poisson-like behavior for larger system sizes is observed, indicating a finite localization length of the eigenstates. The present size-independence of the LSD is compatible with multifractal and extended states.

In conclusion, we have shown that the energy level statistics of TB Hamiltonians defined on the octagonal tiling with different boundary shapes is very well described by RMT. We can even see that our data fit the exact integrated LSD $I_{\rm GOE}(s)$ better than the integrated Wigner surmise $I_{\rm W}(s)$. This supports the applicability of RMT for such completely deterministic Hamiltonians. Although there is no randomness in these quasiperiodic models, one may view the absence of translational symmetry as a sort of "topological disorder". We clarify previous statements [23–25] and show that the universal LSD for irreducible blocks of a symmetric patch, or for patches without any symmetry is always $I_{\rm GOE}(s)$. For patches with the full D_8-symmetry, we find an integrated LSD which is a superposition of seven $I_{\rm GOE}(s)$. Besides the octagonal tiling, we have also considered planar 10- and 12-fold quasiperiodic tilings and found analogous results. In all these cases, we never find a critical $I_c(s)$, distinct from $I_{\rm GOE}(s)$ and $I_{\rm P}(s)$, as observed at the Anderson MIT [9]. This is somewhat surprising since eigenstates in these quasiperiodic tilings are multifractal similarly to states at the MIT, and we could have expected that this is reflected in the LSD. Instead, we find that the LSD is similar to the LSD on the metallic side of the MIT.

We thank M. Baake and I. K. Zharekeshev for discussions. JXZ is grateful for the kind hospitality in Chemnitz. Support from DFG (UG), SFB393 (RAR), SEdC and the National Natural Science Foundation of China (JXZ) is gratefully acknowledged. We dedicate this work to Hans-Ude Nissen, one of the co-discoverers of quasicrystals, on the occasion of his 65th birthday.

[1] E. P. Wigner, Proc. Cambridge Philos. Soc. **47**, 790 (1951); F. J. Dyson, J. Math. Phys. **3**, 140 (1962).
[2] M. L. Mehta, *Random Matrices*, 2nd ed. (Academic Press, Boston, 1990); F. Haake, *Quantum Signatures of Chaos*, 2nd ed. (Springer, Berlin, 1992).
[3] K. B. Efetov, Adv. Phys. **32**, 53 (1983).
[4] O. Bohigas, M. J. Giannoni, and C. Schmit, Phys. Rev. Lett. **52**, 1 (1984).
[5] G. Casati (ed.), *Chaotic Behavior in Quantum Systems: Theory and Application* (Plenum Press, New York, 1985).
[6] B. L. Alt'shuler and B. I. Shklovskii, Zh. Eksp. Teor. Fiz. **91**, 220 (1986) [Sov. Phys. JETP **64**, 127 (1986)];
[7] B. I. Shklovskii, B. Shapiro, B. R. Sears, P. Lambrianides, and H. B. Shore, Phys. Rev. B **47**, 11487 (1993).
[8] E. Hofstetter and M. Schreiber, Phys. Rev. B **48**, 16979 (1993); Phys. Rev. B **49**, 14726 (1994); Phys. Rev. Lett. **73**, 3137 (1994).
[9] I. K. Zharekeshev and B. Kramer, Phys. Rev. Lett. **79**, 717 (1997).
[10] M. Schreiber and H. Grussbach, Phys. Rev. Lett. **67**, 607 (1991).
[11] T. Fujiwara and H. Tsunetsugu, in: *Quasicrystals: The State of the Art*, eds. D. P. DiVincenzo and P. J. Steinhardt (World Scientific, Singapore, 1991), pp. 343–360.
[12] T. Rieth, U. Grimm, and M. Schreiber, to appear in: Proceedings of ICQ6, eds. S. Takeuchi and T. Fujiwara (World Scientific, Singapore, 1997).
[13] D. Mayou, in: *Lectures on Quasicrystals*, eds. F. Hippert and D. Gratias (Les Editions de Physique, Les Ulis, 1994), pp. 417–462; C. Berger, *ibid.*, pp. 463–504.
[14] D. Shechtman, I. Blech, D. Gratias, and J. W. Cahn, Phys. Rev. Lett. **53**, 1951 (1984).
[15] T. Ishimasa, H.-U. Nissen, and Y. Fukano, Phys. Rev. Lett. **55**, 511 (1985).
[16] L. Bendersky, Phys. Rev. Lett. **55**, 1461 (1985).
[17] N. Wang, H. Chen, and K. H. Kuo, Phys. Rev. Lett. **59**, 1010 (1987).
[18] C. Janot, *Quasicrystals — a Primer*, 2nd ed. (Clarendon Press, Oxford, 1994).
[19] M. Kohmoto and B. Sutherland, Phy. Rev. Lett. **56**, 2740 (1986); M. Arai, T. Tokihiro, M. Kohmoto, and T. Fujiwara, Phys. Rev. B **37**, 2797 (1988); T. Rieth and M. Schreiber, Phys. Rev. B **51**, 15827 (1995).
[20] Y. Liu and P. Ma, Phys. Rev. B **43**, 1378 (1991).
[21] C. Sire and J. Bellissard, Europhys. Lett. **11**, 439 (1990); J. X. Zhong and R. Mosseri, J. Phys. (France) I **4**, 1513 (1994).
[22] B. Passaro, C. Sire, and V. G. Benza, Phys. Rev. B **46**,

13751 (1992).
[23] V. G. Benza and C. Sire, Phys. Rev. B **44**, 10343 (1991).
[24] F. Piéchon and A. Jagannathan, Phys. Rev. B **51**, 179 (1995).
[25] J. X. Zhong and H. Q. Yuan, to appear in: Proceedings of ICQ6, eds. S. Takeuchi and T. Fujiwara (World Scientific, Singapore, 1997).
[26] R. Ammann, B. Grünbaum, and G. C. Shephard, Discrete Comput. Geom. **8**, 1 (1992); M. Duneau, R. Mosseri, and C. Oguey, J. Phys. A **22**, 4549 (1989); M. Baake and D. Joseph, Phys. Rev. B **42**, 8091 (1990).
[27] A. Katz, in: *Beyond Quasicrystals* (Springer, Berlin, 1995), pp. 141–189.
[28] K. Müller, B. Mehlig, F. Milde, and M. Schreiber, Phys. Rev. Lett. **78**, 215 (1997).

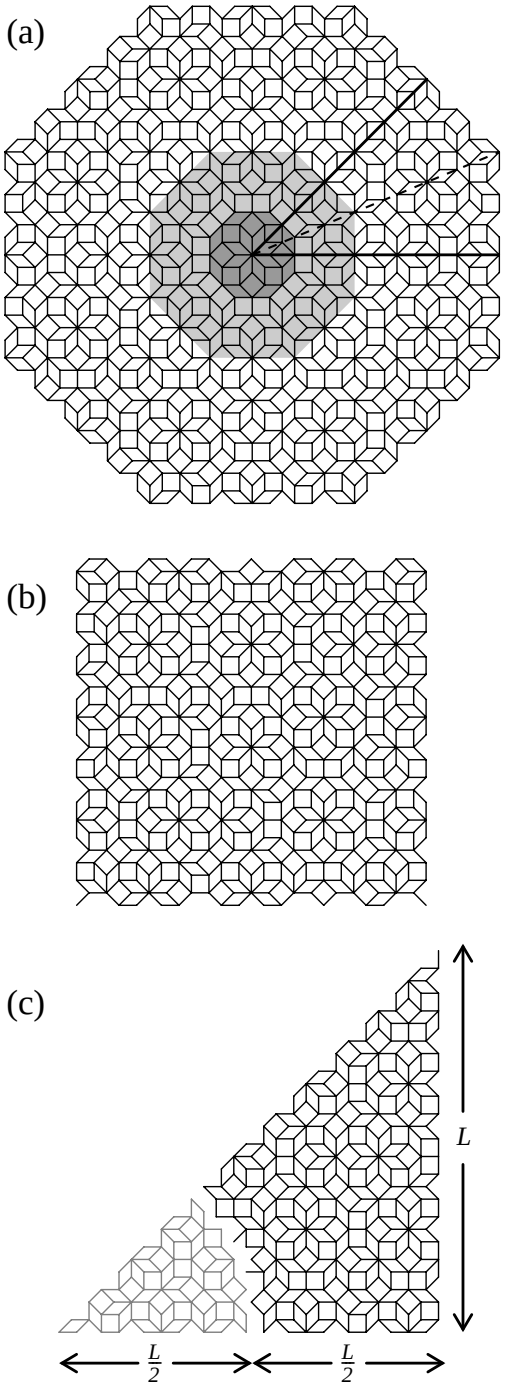

FIG. 1. (a) Octagonal cluster of the Ammann-Beenker tiling with exact eightfold rotational symmetry around the central vertex $(x, y) = (0, 0)$ as indicated by the solid and dashed lines. Shadings indicate successive inflation steps of the central octagon. The patch contains 833 vertices. (b) Square-shaped cut defined by $0 \le x \le L$, $-\frac{L}{4} \le y \le \frac{3L}{4}$ with $L = 20$ with 496 vertices. (c) Sinai billiard-shaped patch defined by $0 \le y \le x \le L$ and $x^2 + y^2 \ge \frac{L^2}{4}$ with $L = 22$ with 246 vertices. The gray edges correspond to the interior of the circular arc; edges crossing the arc have been deleted.

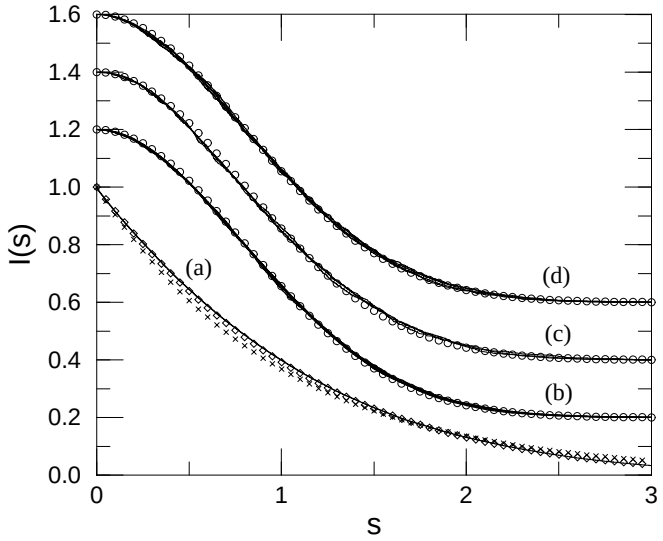

FIG. 2. Integrated LSD $I(s)$ for (a) the largest D_8-symmetric octagonal patch, crosses ($\times$) indicate $I_{\rm P}(s)$, diamonds ($\diamond$) indicate $I_{\rm W}^{(7)}(s)$; (b) the seven independent subspectra of the largest D_8-symmetric octagonal patch, circles ($\circ$) indicate $I_{\rm W}(s)$; (c) squared-shaped patches of different sizes, circles as in (b); (d) Sinai billiard-shaped patches of different sizes, circles as in (b). Curves (b)–(d) have been shifted by multiples of 0.2 for clarity.

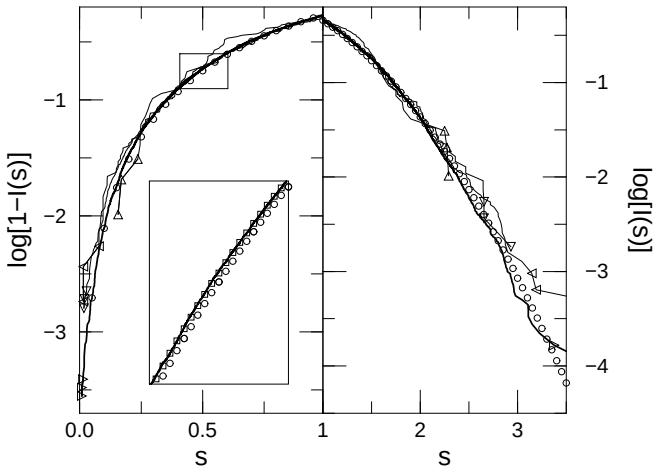

FIG. 3. Small-s (left) and large-s (right) behavior of $I(s)$ for one irreducible sector of D_8-symmetric octagonal patches of different sizes. The bold line corresponds to the largest patch. The three smallest and largest level spacings for each patch are denoted by triangles of different orientations. The circles ($\circ$) indicate $I_{\rm W}(s)$. Inset: blow-up of the data region enclosed by the rectangle, showing only data for the largest patch. Squares ($\Box$) indicate $I_{\rm GOE}(s)$.